Available online at www.sciencedirect.com
ScienceDirect
Trans. Nonferrous Met. Soc. China 22(2012) 1264−1269
Transactions of Nonferrous Metals Society of China
www.tnmsc.cn

Growth mechanism of primary silicon in cast hypoeutectic Al−Si alloys

WANG Shou-ren[1], MA Ru[1], WANG Ying-zi[2], WANG Yong[3], YANG Li-ying[1]

1. School of Mechanical Engineering, University of Jinan, Ji'nan 250022, China;
2. School of Materials science and Engineering, University of Jinan, Ji'nan 250022, China;
3. School of Physics Science, University of Jinan, Ji'nan 250022, China

Received 24 June 2011; accepted 30 September 2011

Abstract: The microstructural features of hypoeutectic Al−10%Si alloy were observed using optical microscopy and electron backscatter diffraction. The results show that primary silicon particles are frequently found in hypoeutectic alloys. Hence, the nucleation and growth mechanisms of the precipitation of primary silicon of hypoeutectic Al−10%Si alloy melts were investigated. It was discovered that Si atoms are easy to segregate and form Si−Si clusters, which results in the formation of primary silicon even in eutectic or hypoeutectic Al−Si alloys. In addition, solute redistribution caused by chemical driving force and large pile-ups or micro-segregation of the solute play an important role in the formation of the primary silicon, and the solute redistribution equations were derived from Jackson-Chalmers equations. Once Si solute concentration exceeds eutectic composition, primary silicon precipitates are formed at the front of solid/liquid interface.

Key words: Al−Si alloys; solidification; crystal growth; primary silicon; solute redistribution

1 Introduction

Aluminum−silicon alloys have been widely used in structural applications of aerospace and automobile industries due to their low thermal expansion coefficients, high wear resistance and good cast ability [1,2]. Al−Si alloys can be classified into three groups according to the silicon content, hypoeutectic, eutectic and hypereutectic alloys. Each group has silicon content of less than 10%, 11% to 13%, and more than 14%, respectively. According to the Al−Si binary phase diagram, eutectic reaction occurs at eutectic temperature. Two solid phases (eutectic silicon Si_E and α(Al)) simultaneously crystallize from the liquid phase (L) with an eutectic composition of 12.6% Si, via the reaction of $L \longrightarrow Si_E+\alpha(Al)$. For hypoeutectic Al−Si alloys, crystallization of the α(Al) phase is followed by eutectic reaction. The reaction for hypoeutectic alloy is $L \longrightarrow L+\alpha(Al) \longrightarrow (Si_E+\alpha(Al))+\alpha(Al)$. Hypereutectic Al−Si alloy shows the primary crystallization of silicon precipitates, and then the eutectic reaction comes after the primary silicon. Hypereutectic reaction generally exhibits the following phase transformation as: $L \longrightarrow L+Si_P \longrightarrow (Si_E+\alpha(Al))+Si_P$, where Si_P is the primary silicon.

According to the Al−Si binary phase diagram, primary silicon particles (PSPs) are precipitated only from hypereutectic Al−Si alloy melts. Many PSPs, however, are experimentally found in hypoeutectic alloys. The following phase transformation is suggested for hypoeutectic Al–Si alloys as: $L \longrightarrow L+\alpha(Al) \longrightarrow L+\alpha(Al)+Si_p \longrightarrow (Si_E+\alpha(Al))+\alpha(Al)+Si_p$. The PSPs have sharp edges and flat faces, which are the facet characteristics. They possess various size and morphology with a strong trend toward the predominance of octahedral crystals faced by {111} facets [3−5]. Although numerous literatures [6−8] have analyzed and predicted the morphology using crystal growth theories of the PSPs, very little information is available concerning the nucleation and growth features of the PSPs in hypoeutectic Al−Si alloys. The present study discussed the reason why PSPs occur in hypoeutectic Al−Si alloys. The nucleation and growth mechanisms of PSPs were also presented.

Foundation item: Project (U1134101) supported by the Mutual Foundation of Basic Research of High Speed Railway, China; Projects (ZR2009FL003, ZR2010EL011, ZR2011EMM003) supported by the Natural Science Foundation of Shandong Province, China
Corresponding author: WANG Shou-ren; Tel: +86-531-82765476; Fax: +86-531-87108467; E-mail: sherman0158@tom.com
DOI: 10.1016/S1003-6326(11)61314-9

2 Experimental

The rapid solidification experimental procedures were as followings. First, the Al−Si alloy ingot was placed in an induction furnace to melt: The temperature of the furnace was set at 715 °C, then this temperature was kept for 2 min to stabilize and homogenize the melt. Next, the melt was cooled to the pouring temperature and then rapidly solidified to room temperature. A controlled flow of compressed gas and/or atomized sprayed water was used to obtain high cooling rate. The curves of solidification temperature and cooling time shown in Fig. 1 were automatically calculated and plotted. As shown in Fig. 1, the cooling rates of 4 different samples with thickness of 20, 40, 60 and 80 mm were calculated as 3.8, 6.6, 9.8 and 16.1 °C/s, respectively.

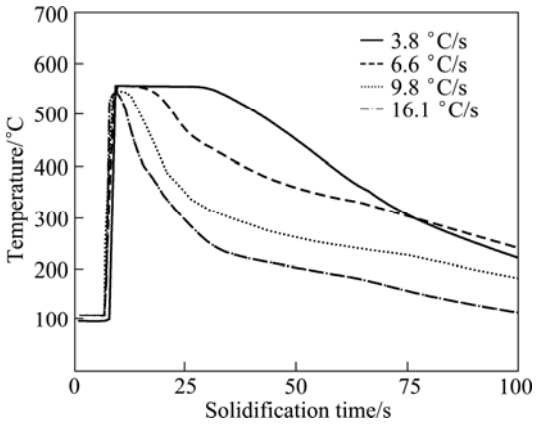

Fig. 1 Relationship of solidification temperature and cooling time

The composition of the alloys used in this study was Al−10%Si. In order to eliminate the influence of impurities, the melt needs to be refined. Samples for micrograph observation were mounted in a holder and polished using SiC papers (up to 2000 grit). The optical microstructures were observed after mechanical polishing with glycol based polycrystalline diamond suspension. Microstructural features of primary silicon were investigated using electron backscatter diffraction (EBSD). The EBSD specimens were prepared by both mechanical and electro polishing. The electro polishing was made at 20 V for about 20 s in a solution of ethanol and perchloric acid (6:1) at −15 °C. EBSD data were acquired using a JEOL JSM−7001F field emission scanning electron microscope (FE-SEM) with the HKL Channel 5 EBSD software (HKL Technology, Denmark). The FE-SEM was operated at 20 kV in a high vacuum mode and specimens were tilted at 70°. For the two-dimensional (2D) observations of PSPs, Al−Si samples were etched using a 40% $HClO_4$ dilute solution. The 2D microstructures were characterized using a scanning electron microscope (SEM) equipped with an energy dispersive spectroscopy (EDS). For the observation of three-dimensional (3D) features of octahedral primary silicon, samples were deep-etched with the same solution.

3 Results

It is found that lots of primary Si particles (PSPs) occur in the hypoeutectic Al−Si alloy, as shown in Fig. 2. From Fig. 2, it is shown that with the increasing cooling rate, the amount and the size of PSPs are both reduced. The equivalent diameter of PSPs is reduced from approximately 88.9 to 17.1 μm when the average cooling rate increases from 3.8 to 16.1 °C/s. In addition, the distribution of PSPs is non-homogenous no matter the cooling rate is higher or lower.

The micrographs of hypoeutectic Al−10%Si alloys measured by SEM/EDS are displayed in Fig. 3. All α(Al), Si_P and Si_E are found in Fig. 3(a). Particularly, EDS mapping confirms that there exist both Si_E and faceted Si_P particles in hypoeutectic Al−Si alloys (Fig. 3(b)). The 3D microstructures measured by deep-etching method are shown in Figs. 3(c) and (d). The faceted PSPs are surrounded by α(Al) dendrites and Si/Al eutectic phases. Eutectic silicon connected to the PSPs is broken in an ethanol bath by using an ultrasonic cleaner. Owing to the dissolution of the α(Al) matrix, the PSPs are partly or fully extracted from the α(Al) matrix without damage to their surfaces and edges, and they exhibit perfect (Fig. 3(c)) or imperfect (Fig. 3(d)) octahedral structures.

Dislocations promoting continuous spiral growth (DPCS) and twin plane re-entrant edge (TPRE) growth mechanism are suggested for the growth modes of PSPs in hypereutectic alloys [8]. The growth mechanisms of faceted PSPs in hypoeutectic alloys seem to be similar to those of hypereutectic alloys. Fine grooves can be seen on the faces and the facets (as marked by arrows in Fig. 3(c)), and they look like the traces of growth steps that are at an oblique angle to the groove or to the ridge. The stable groove maintaining on the surface of a twinned crystal facilitates rapid growth of the faceted PSPs in the specific direction [3].

A primary silicon particle shown in Fig. 4 displays a five petal growth characteristic based on TPRE growth mechanism. The PSPs consist of five successive twins representing in different colors. The adjoining two facets usually have a twin relationship, 60°⟨111⟩. It is also found that two parallel twin planes produce a self-perpetuating system of 141° groove (Fig. 4(b)), in which nucleation occurs readily. Five silicon tetrahedrons are assembled along the perfect ⟨112⟩ orientation in the {111} twining planes which are indexed in Fig. 4(c).

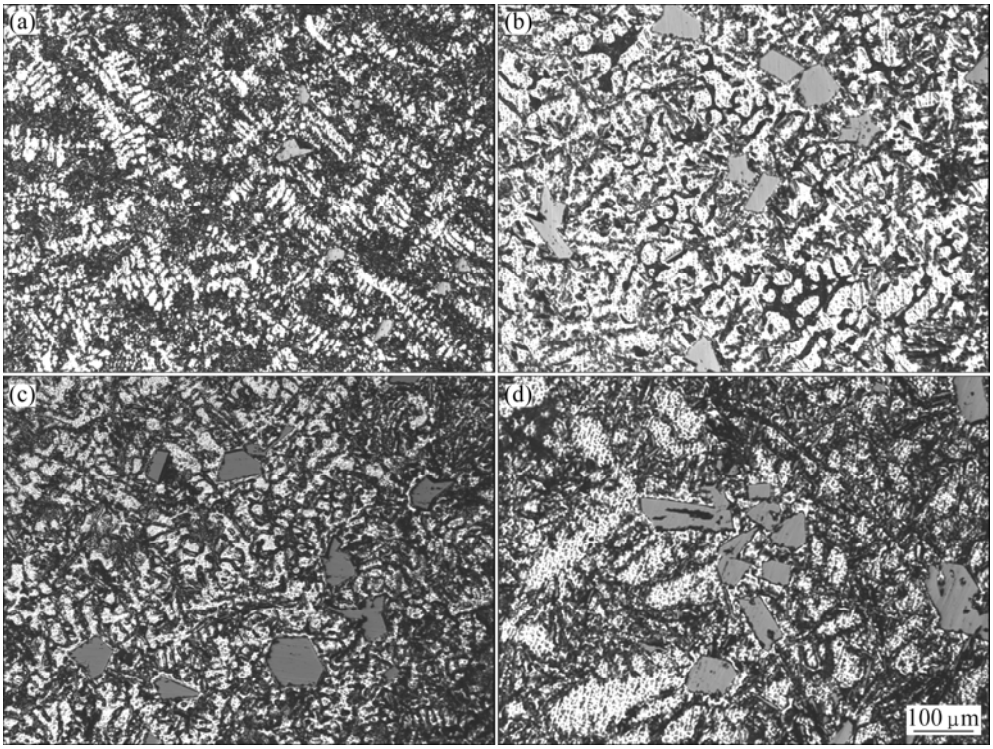

Fig. 2 OM images of Al−10%Si alloys at different cooling rates: (a) 16.1 ºC/s; (b) 9.8 °C/s; (c) 6.6 °C/s; (d) 3.8 °C/s

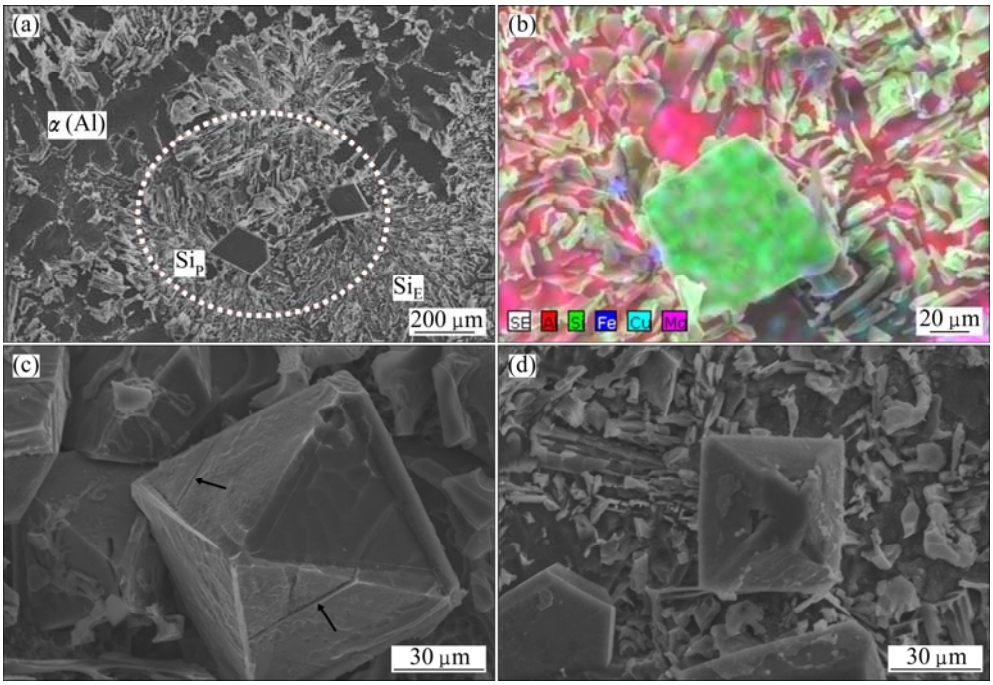

Fig. 3 SEM images of hypoeutectic Al−10%Si alloys showing 2D microstructure (a), EDS mapping and Si_P showing 3D features (b), perfect octahedral primary silicon (c) and imperfect octahedral primary silicon (d)

4 Discussion

PSPs are frequently found in hypoeutectic alloys, as measured above. Investigations on nucleation and growth of the PSPs provide some reasons why they form in hypoeutectic alloys. According to the solidification features of Al−Si alloys, Si atoms are easy to segregate and form Si clusters, which have a large tendency to nucleate and grow at the liquid/solid interface front. Some researchers [9−12] have suggested that there are Si clusters and Si tetrahedrons in the melt of Al−Si alloys,

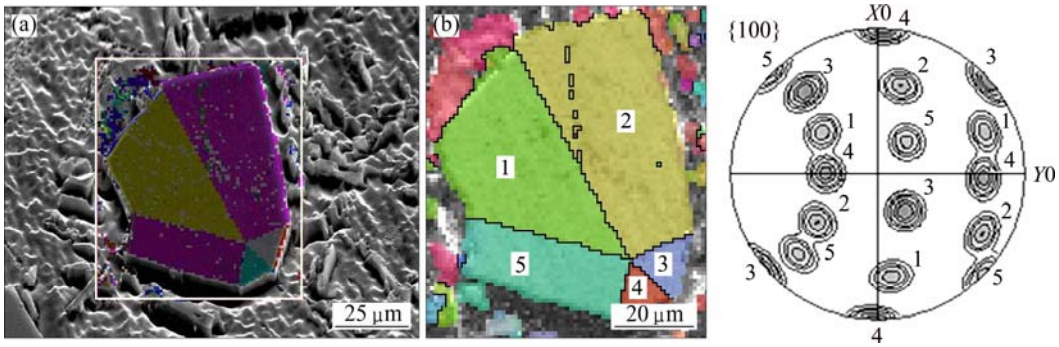

Fig. 4 SEM image of Al−10%Si alloy showing primary silicon particle (a), orientation imaging micrograph (b) and {100} pole figure (c)

and such liquid structures should be beneficial for the formation and growth of the nuclei of the PSPs. The Bletry geometrical model [10] supposed that the segregation of Si atoms in the liquid of binary Al−Si alloys can be explained by using the first-neighbor order parameter ξ as:

$$\xi = 1 - \frac{\eta_{12}}{\eta_1 c_2} = 1 - \frac{\eta_{21}}{\eta_2 c_1} \quad (1)$$

where η_1 is the total number of close-contact neighbors to a component-1 atom; η_2 is that to a component-2 atom; η_{12} is the average number of component-2 atoms that are close-contact neighbors to a component-1 atom; η_{21} is that of component-1 atoms to a component-2 atom; c_2 is the atomic concentration of component-2 and c_1 is that of component-1. If ξ>0, the solute atoms are randomly distributed; correspondingly, if ξ<0, the solute atoms make chemical compounds with solvent. Regarding to Al−Si alloys, Si atoms tend to segregate, thus positive first-neighbor order parameter, ξ>0, is reasonable.

As known, the α(Al)/liquid interface is rough and the Si_P/liquid interface is smooth (faceted). The faceted interface grows faster than the rough interface, because the growth of the faceted interface is faster along the preferred directions due to the availability of steps and ledges. Unlike eutectic reactions commonly displaying lamellar structures, the growth of PSPs is not coupled with α(Al). The PSPs follow a random growth mode preceding the growth of the eutectic.

Crystal growth is affected by not only heat transfer but also solute redistribution which results in segregation or compositional inhomogeneity during solidification. Under equilibrium conditions, a distribution coefficient, k_0, is defined as k_0=(C_S/C_L), where C_S and C_L are the solute concentrations in the solid and liquid phases at a given temperature T, respectively. Depending on the original alloy composition and the slopes of the solidus and liquidus lines in the Al−Si phase diagram, k_0<0. Owing to the small solubility of Si in Al matrix (the maximum of solubility is (1.5±0.1)% at 577.6 ºC), the liquid surrounded by the first-formed solid phase, α(Al), becomes enriched with Si solute. That is, the excess Si solute is rejected from the solid phase into the liquid ahead of the growth front. The excess Si solute can migrate to the low-solute area by diffusion through the liquid, or be redistributed by both diffusion and convection, or be homogeneously redistributed throughout the liquid via convection, or form a new solid phase once its concentration exceeds a critical value.

The schematic diagrams in Fig. 5 illustrate four different mechanisms regarding solute redistribution at the solid/liquid interface. TILLER et al [13] assumed that the diffusion in the solid was negligible, and thus the diffusion in the liquid was only considered in Case I (Fig. 5(a)). The solute distribution in the liquid is governed by Fick's second equation [14] as:

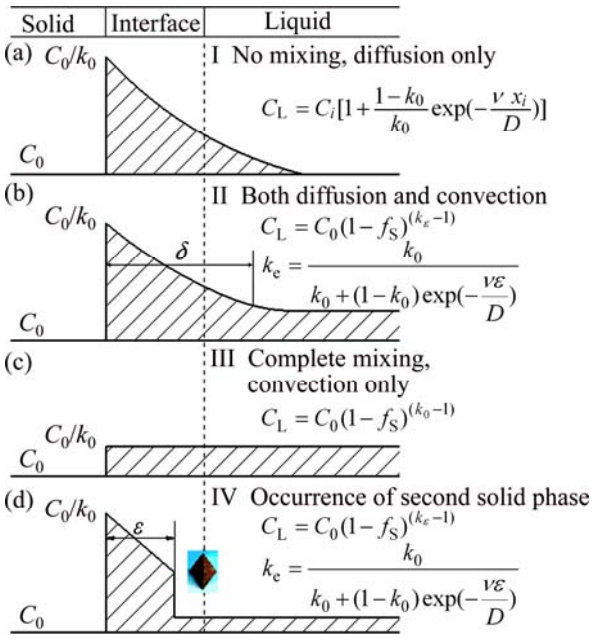

Fig. 5 Solute redistribution at solid/liquid interface: (a) Diffusion only; (b) Both diffusion and convection; (c) Convection only; (d) Occurrence of second solid phase

$$\frac{\partial C}{\partial t} = D\frac{\partial^2 C}{\partial x^2} \tag{2}$$

According to the Fick's equation, the Jackson-Chalmers equation [15] becomes

$$C_{\mathrm{L}} = C_0[1+\frac{1-k_0}{k_0}\exp(-\frac{v x_i}{D})] \tag{3}$$

where C_0 is the solute composition in the bulk liquid phase; D is the diffusion coefficient and v is the growth velocity. Equation (3) describes the variation of the solute composition ahead of the solidification front, and it indicates that a steeper concentration gradient develops at high growth speed v and low solute diffusivity D.

In Case II (Fig. 5(b)), Si solute redistribution is controlled by both diffusion and convection. The solute rich boundary with a thickness layer of δ, located in front of the solidification interface is gradually broken down by the convection driven by temperature gradients. The solute concentration in the liquid phase for Case II is derived and given as:

$$C_{\mathrm{L}} = C_0(1-f_{\mathrm{s}})^{(k_{\mathrm{e}}-1)} \tag{4}$$

where f_{s} is the solid fraction; k_{e} is the effective partition coefficient defined as:

$$k_{\mathrm{e}} = \frac{k_0}{k_0+(1-k_0)\exp(-\frac{v\delta}{D})} \tag{5}$$

A complete solute mixing occurs in Case III (Fig. 5(c)) due to fluid convection. Si solute is rejected from the solid phase for limited solubility during solidification, and it is homogeneously redistributed throughout the liquid. The solute concentration in the liquid for Case III is derived as:

$$C_{\mathrm{L}} = C_0(1-f_{\mathrm{s}})^{(k_0-1)} \tag{6}$$

However, it is difficult to apply the three cases mentioned above (purely diffusive, purely convective or mixed) directly during the solidification of Al−Si alloys. In the binary Al−Si alloys, there exists another solid phase, $\mathrm{Si_P}$, in addition to α(Al). The formation of the second solid phase during solidification affects the solute concentration, particularly near the solid/liquid interface. A solute distribution curve with both α(Al) and $\mathrm{Si_P}$ is suggested as Case IV (Fig. 5(d)) to have a similar profile to Case II except a sharp decrease in the concentration in the liquid side. The solute rich boundary layer with a thickness of ε, ahead of the solidification interface is abruptly broken down by the formation of a new second phase. The solute concentration equation in the liquid for Case IV is similar to Eq. (4), except the effective partition coefficient, k_{e}, which is defined as:

$$k_{\mathrm{e}} = \frac{k_0}{k_0+(1-k_0)\exp(-\frac{v\varepsilon}{D})} \tag{7}$$

Under this condition, the first solid phase, α(Al), continues to form from the melts and the surrounding liquid progressively becomes rich in Si solute. Large pile-ups or micro-segregation of the solute can locally occur at the solid/liquid interface. Once the solute concentration at the interface exceeds a critical value, eutectic composition (C_{E}), the second solid phase $\mathrm{Si_P}$ would precipitate at the solid/liquid interface.

The variations of the solute concentration at the solidification front with both α(Al) and $\mathrm{Si_P}$ are shown in Fig. 6. During solidification, Al atoms rejected by Si diffuse through the liquid toward the liquid/α(Al) interface, and they are incorporated into the α(Al) phase. Similarly, Si atoms rejected by Al diffuse toward the liquid/Si interface, and they form a cluster of Si atoms in the liquid. The concentration of Si clusters increases with solidification time and once it exceeds C_{E}, the PSPs are shaped from the liquid. This results in a sharp decrease of Si concentration in the solute rich boundary layer with a thickness of ε_1. With the solid/liquid interface gradually proceeding, Si clustering repeats the procedure. The concentration of Si clusters increases again, and then the second solute rich boundary layer with a thickness of ε_2 begins to form. In this way, PSPs can be continually precipitated at the moving front of solidification interface, in addition to α(Al).

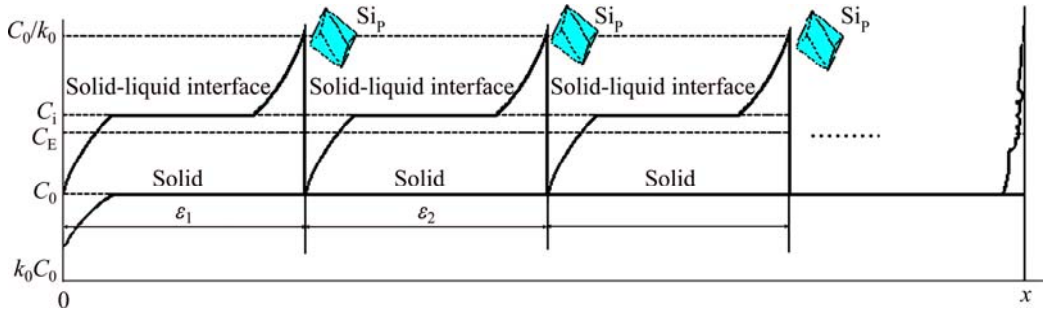

Fig. 6 Repeated variations of solute concentration at solidification boundary

5 Conclusions

1) The micrographs of hypoeutectic Al−Si alloys are observed, and the primary silicon particles are frequently found in the alloys. The equivalent diameter and the amount of the PSPs in hypoeutectic alloys are both reduced with increasing cooling rate; in addition, the PSPs exhibit octahedral structures.

2) The growth mechanisms of faceted PSPs in hypoeutectic alloys seem to be twin plane re-entrant edge growth mechanism. The PSPs follow a random growth mode preceding the growth of the eutectic.

3) Solute redistribution plays an important role in the formation of PSPs, and there are four different solute redistribution mechanisms. Once the Si solute concentration at the solid/liquid interface exceeds the eutectic composition, the primary silicon precipitates would form during the solidification of hypoeutectic Al−Si alloy.

References

[1] SINGH H, GOKHALE A M, TEWARI A, ZHANG S, MAO Y. Three-dimensional visualization and quantitative characterization of primary silicon particles in an Al−Si base alloy [J]. Scripta Mater, 2009, 61(4): 441−444.

[2] El SEBAIE O, SAMUEL A M, SAMUEL F H, DOTY H W. The effects of mischmetal, cooling rate and heat treatment on the eutectic Si particle characteristics of A319.1, A356.2 and A413.1 Al–Si casting alloys [J]. Mater Sci Eng A, 2008, 480(1−2): 342−355.

[3] WANG R Y, LU W H, HOGAN L M. Faceted growth of silicon crystals in Al−Si alloys [J]. Metall Mater Trans A, 1997, 28(5): 1233−1243.

[4] LI C, WU Y Y, LI H, LIU X F. Morphological evolution and growth mechanism of primary Mg_2Si phase in Al−Mg_2Si alloys [J]. Acta Mater, 2011, 59(3): 1058−1067.

[5] SINGH H, GOKHALE A M, TEWARI A, ZHANG S, MAO Y. Three-dimensional visualization and quantitative characterization of primary silicon particles in an Al–Si base alloy [J]. Scripta Mater, 2009, 61(4): 441−444.

[6] PEI Y T, DE HOSSON J T M. Five-fold branched Si particles in laser clad AlSi functionally graded materials [J]. Acta Mater, 2001, 49(4): 561−571.

[7] LU D H, JIANG Y H, GUAN G S, ZHOU R F, LI Z H, ZHOU R. Refinement of primary Si in hypereutectic Al–Si alloy by electromagnetic stirring [J]. J Mater Process Tech, 2007, 189(1−3): 13−18.

[8] XU C L, WANG H Y, LIU C, JIANG Q C. Growth of octahedral primary silicon in cast hypereutectic Al−Si alloys [J]. J Cryst Growth, 2006, 291(2): 540−547.

[9] GREMAND M, ALLEN D R, RAPPAZ M, PEREPEZKO J H. The development of nucleation controlled microstructures during laser treatment of Al−Si alloys [J]. Acta Mater, 1996, 44(7): 2669−2681.

[10] SYLVAN Z B. Liquid metals chemistry and physics [M]. New York: Chem & Phys, M D Inc, 1972: 164−170.

[11] XU C L, JIANG Q C. Morphologies of primary silicon in hypereutectic Al–Si alloys with melt overheating temperature and cooling rate [J]. Mater Sci Eng A, 2006, 437(2): 451−455.

[12] LI P J, NIKITIN V I, KANDALOVA E G, NIKITIN K V. Effect of melt overheating, cooling and solidification rates on Al–16 wt.% Si alloy structure [J]. Mater Sci Eng A, 2002, 332(1−2): 371−374.

[13] TILLER W A, JACKSON K A, RUTTER J W, CHALMERS B. The redistribution of solute atoms during the solidification of metals [J]. Acta Mater, 1953, 1(4): 428−437.

[14] DOHERTY R D. Diffusive phase transformations in the solid state [M]. New York: Physical Metallurgy, 1996: 1363−1368.

[15] WANG W M, BIAN X F, QIN J Y, SYLIUSARENKO S I. The atomic-structure changes in Al−16 pct Si alloy above the liquidus [J]. Metall Meter Trans A, 2000, 31(9): 2163−2168.

铸态亚共晶 Al−Si 合金中初生硅的生长机制

王守仁[1], 马 茹[1], 王英姿[2], 王 勇[3], 杨丽颖[1]

1. 济南大学 机械工程学院，济南 250022；
2. 济南大学 材料科学与工程学院，济南 250022；
3. 济南大学 物理科学学院，济南 250022

摘 要：利用光学显微镜和电子背散射衍射技术观察亚共晶 Al−10%Si 合金的微观结构特征。结果表明, 在亚共晶合金内很容易发现初生硅颗粒。研究亚共晶 Al−10%Si 合金溶液中初生硅析出过程中的晶核形成和生长机制，发现硅原子容易偏析并形成 Si−Si 簇，即使在共晶和亚共晶合金内，这一现象也会导致初生硅的形成。另外，由化学驱动力和较大的堆积碰撞或溶质的凝固偏析等原因引起的溶质再分配在初生硅的形成过程中也起着重要的作用，其中溶质再分配方程由 Jackson-Chalmers 方程推导而出。一旦硅溶质浓度超过共晶成分，在固/液界面的前端就会析出初生硅。

关键词：Al−Si 合金；凝固；晶粒生长；初生硅；溶质再分配

(Edited by FANG Jing-hua)